

Cyclic liquefaction resistance of sand under a constant inflow rate

O. ADAMIDIS* & I. ANASTASOPOULOS†

Cyclic resistance curves, derived through undrained element tests, are central to the study of liquefaction. Their use implies that water drainage is negligible during an earthquake. Nevertheless, a growing body of evidence suggests that this hypothesis is not realistic. In proximity to the interface of a liquefiable layer with an overlying lower permeability layer, upwards water flow can lead to localised, co-seismic pore volume increase. This paper aims to quantify the effects of pore volume increase on cyclic resistance curves. Cyclic triaxial experiments are presented, performed under undrained conditions and under conditions of volumetric expansion. A constant inflow rate is chosen for the sake of simplicity. Results show that even small inflow rates have a detrimental effect on cyclic resistance. A simplified methodology is developed, which can estimate cyclic resistance under constant water inflow rates, by assuming a superposition of isotropic unloading and undrained cyclic shearing. The presented results add to increasing evidence on how current liquefaction susceptibility assessments might not be conservative for layered deposits. In addition, they highlight significant aspects of soil response under partially drained conditions.

KEYWORDS: Liquefaction, Partial drainage, Liquefaction resistance, Triaxial tests, Cyclic triaxial testing, Hostun sand

INTRODUCTION

The undrained hypothesis has been at the core of earthquake-induced liquefaction understanding since research on the subject began. It states that during an earthquake, there is not sufficient time for water flow to cause void redistribution, thus justifying a constant volume, undrained condition at an element level. The convenience of imposing undrained conditions in testing apparatuses facilitated the proliferation of such results. Starting with the work of Castro (1969), undrained element tests were extensively used to create frameworks that describe and classify the response of liquefiable materials subjected to monotonic or cyclic loading (e.g., Ishihara *et al.*, 1975; Luong & Sidaner, 1981; Been & Jefferies, 1985; Ishihara, 1985; Konrad, 1993; Ishihara, 1993).

A particularly consequential methodology, based on undrained element testing, is the simplified stress based approach for the evaluation of the liquefaction potential of a deposit, proposed by Seed & Idriss (1967). This methodology uses series of cyclic undrained element tests, performed at a given relative density and initial confinement, to create ‘cyclic resistance curves’, where the number of cycles required for liquefaction is given as a function of the amplitude of cyclic shearing. When performing an assessment for a certain design earthquake using this methodology, a characteristic earthquake-induced stress is defined and the earthquake load is converted to an equivalent load of uniform cycles of the characteristic stress. Using the cyclic resistance curve and the number of equivalent cycles for the design earthquake, the stress required to cause liquefaction is calculated and compared to the characteristic earthquake-induced stress. If found to be lower, the examined deposit is deemed susceptible to liquefaction at the examined depth.

Practising engineers nowadays use updated methods for the assessment of liquefaction susceptibility, which still - directly or indirectly - depend on the undrained hypothesis. The most commonly used methods are evolutions of the stress based

approach of Seed & Idriss (1967). In Boulanger & Idriss (2014) and Boulanger & Idriss (2016), the resistance to liquefaction is estimated using an in-situ parameter, such as CPT penetration resistance or SPT blow count, and applying statistical models stemming from an extended database of case histories; an approach initiated by Seed *et al.* (1983). Though no longer directly using undrained cyclic resistance curves, the current method still does not account for any potential effects of localised void redistribution due to the presence of layers of different permeability. Alternatively to the stress based method, energy based approaches have also been proposed (e.g. Berrill & Davis, 1985; Kokusho, 2013). These depend on undrained element tests to relate energy dissipation to excess pore water pressure generation in a unique way, an assumption first proposed by Nemat-Nasser & Shokoh (1979). Finally, evaluations for a deposit can be performed numerically, using one-dimensional (1D) finite element simulations, preferably with a coupled solid-fluid (u-p) formulation (Zienkiewicz *et al.*, 1980) and constitutive models that can account for excess pore water pressure generation (for example, the model of Prevost (1985) is at the core of such simulations in the software ‘Cyclic 1D’, developed by Elgamal *et al.* (2006)). Constitutive models are calibrated to capture pore pressure generation under undrained conditions, often targeting specific undrained cyclic resistance curves.

Although the undrained hypothesis underpins much of liquefaction research, it is not necessarily appropriate for liquefaction during an earthquake. Working on a general formulation for liquefaction, Goren *et al.* (2010) and Lakeland *et al.* (2014) suggested that fluid flow must have a significant effect on the evolution of excess pore water pressures in the field. Adamidis & Madabhushi (2018b) experimentally confirmed this conclusion using dynamic centrifuge tests. They showed that partially drained conditions are more appropriate for a liquefaction event and that the proximity and nature of drainage boundaries control the evolution of excess pore water pressure.

The necessity of transitioning our view of liquefaction from an undrained to a partially drained event is very pertinent for the problem of liquefaction susceptibility of layered deposits, particularly when examining layers of different permeability, which are currently assessed in isolation. Indeed, Cubrinovski *et al.* (2019) present multiple cases from the 2010–2011

Manuscript received...

* Department of Engineering Science, University of Oxford, Parks Road, Oxford, OX1 3PJ, UK

† IGT, ETH Zurich, 5 Stefano-Francsini Platz, 8093 Zurich, Switzerland

series of Canterbury earthquakes in New Zealand, where a system approach that accounts for interaction between layers is required to provide an accurate assessment of liquefaction occurrence and severity. In particular, they stress the importance of water inflow from underlying layers in liquefaction of the critical layer, as well as the possibility of seepage-induced liquefaction of soils above the water table. Moreover, they show that deep layers overlain by non-liquefiable layers can liquefy rapidly, isolating the rest of the deposit. Tsaparli *et al.* (2020) demonstrate how current simplified liquefaction susceptibility assessments led to a false negative case during the same series of earthquakes, due to not accounting for water drainage that led to void redistribution in proximity to the interface of a liquefiable with a lower permeability layer. The occurrence of localised volumetric expansion below a lower permeability layer, to the point of the formation of a water film, was first identified by Kokusho (1999). Malvick *et al.* (2008), looking at flow failures in slopes, also point out this behaviour and present estimations regarding the magnitude of volumetric expansion that takes place below a low permeability silt layer. Overall, the need for updated liquefaction susceptibility assessments in layered deposits is becoming increasingly evident.

Beyond susceptibility assessment, the implications of viewing liquefaction as a partially-drained phenomenon extend to the behaviour of constitutive models for liquefaction (e.g. Prevost, 1985; Dafalias & Manzari, 2004; Andrianopoulos *et al.*, 2010; Boulanger & Ziotopoulou, 2013; Tasiopoulou & Gerolymos, 2015; Dafalias & Taiebat, 2016). These models are typically developed to simulate undrained response and are calibrated versus undrained element tests. Although numerical simulations often include a coupled solid-fluid (u-p) formulation (Zienkiewicz *et al.*, 1980) that allows drainage, and thus volumetric strains to take place during the earthquake, it is uncertain whether constitutive models calibrated on the basis of undrained conditions perform adequately when volumetric strains are imposed.

To begin addressing these issues, better insight on the behaviour of liquefiable materials under partially drained conditions is required. Few results from monotonic element tests are available, where the ratio of volumetric over axial strain is kept constant (Vaid & Eliadorani, 2000; Eliadorani & Vaid, 2005; Sivathayalan & Logeswaran, 2008; Nicot *et al.*, 2013). These investigations are primarily relevant for post-earthquake failure of slopes due to seepage. However, to the authors knowledge, no data are available on cyclic element tests under specified, non-zero, volumetric expansion rates. Of particular interest is the condition of volume increase due to water inflow, which can occur in proximity to the interface of a liquefiable layer with an overlying layer of low permeability; a condition that is not accounted for by current simplified assessments (Cubrinovski *et al.*, 2019) and can lead to false negative predictions (Tsaparli *et al.*, 2020). This paper makes a first step in addressing such issues, by presenting results from cyclic triaxial experiments under a condition of water inflow. For simplicity, constant rates of water inflow are used. The results are presented in terms of cyclic resistance curves, which are of significance both for liquefaction susceptibility assessments and for constitutive model calibration.

The major contribution of this paper is threefold. Firstly, novel experimental results on the cyclic response of liquefiable material under a constant rate of water inflow are presented. Stemming from non-standard testing, these results demonstrate that even a very small rate of water inflow is sufficient to dramatically reduce the undrained cyclic resistance of a liquefiable deposit. Secondly, a simplified methodology is proposed to quantify the effects of water inflow on cyclic

resistance curves. The developed methodology uses typically available results from standardised testing (the undrained cyclic resistance curve and the isotropic unloading line) to estimate cyclic resistance under a given water inflow rate. The estimations are shown to be accurate for a range of densities and inflow rates. Finally, the experimental data are included as supplementary material, to inform the development and calibration of constitutive models.

EXPERIMENTAL METHODS

The experiments presented herein were performed using the triaxial devices of the ETH Zurich (ETHZ) Institute for Geotechnical Engineering (IGT) (Fig. 1a). These devices allow the performance of monotonic and cyclic triaxial tests, in a stress- or strain-controlled manner. A pore water pressure transducer was connected to each end of the specimen, and a third pore water pressure transducer was connected to the cell. The range of the pressure transducers was 1MPa and the accuracy was 0.15%. Nylon tubing was used for the drainage line. No effects on volume measurement from drainage line compliance were measured for the pressure ranges examined. A detailed description of the triaxial devices is given by Trausch-Giudici (2004).

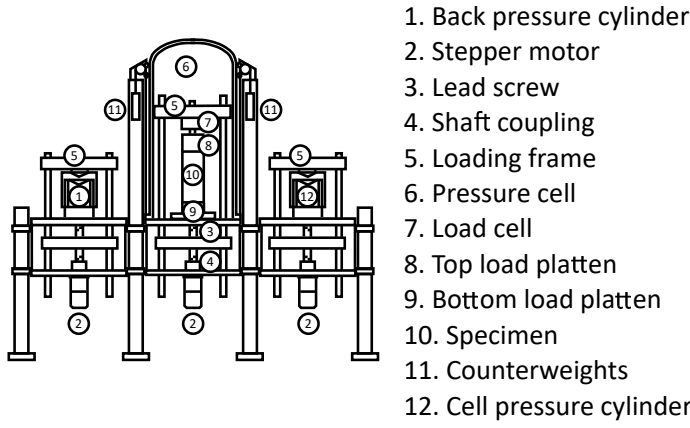
The sand used was Hostun HN31, a sub-angular to angular siliceous sand that is widely used in geotechnical physical modelling in Europe, in particular for liquefaction-related problems (e.g. Adamidis & Madabhushi, 2018a). Its properties are summarised in Table 1. The minimum and maximum void ratios were measured following ASTM D4253-16e1 (2016) and ASTM D4254-16 (2016) respectively. The critical friction angle was calculated from drained triaxial compression experiments. The rest of the properties included in Table 1 are reproduced from Adamidis *et al.* (2020).

Table 1. Properties of Hostun sand. Permeability was measured at a void ratio of $e = 0.836$.

e_{max}	e_{min}	d_{50}	$\frac{d_{60}}{d_{10}}$	G_S	ϕ_{crit}	k
1.049	0.671	341 μm	1.48	2.65	33°	0.92 $\frac{mm}{s}$

Triaxial specimens were prepared in a cylindrical mould of 50 mm diameter and 100 mm height, using water (wet) pluviation. Sand that was fully saturated in de-aired water was pluviated into the membrane lined and de-aired water filled split mould. The sand was densified to the required void ratio by gentle tapping. While filling the triaxial cell with water, the specimen was kept at an effective stress of 5 kPa. A photo of a specimen before testing is shown in Fig. 1b. After filling the cell, a backpressure of 150 kPa was applied. B-value tests yielded values above 95% in all cases. Specimens were isotropically consolidated to a mean effective stress of $p' = 100$ kPa before applying stress-controlled, slow cyclic loading. The testing protocol was based on ASTM D5311/D5311M-13 (2013), using a constant volume condition for the undrained tests and a constant rate of volumetric expansion for the partially drained ones. The volumetric expansion condition was realised by setting the water pressure-volume control cylinder connected to the bottom of the specimen to move at a constant velocity, corresponding to the required constant volumetric strain rate. The movement of the pressure-volume control cylinder was triggered with the start of cyclic loading.

The condition of volumetric expansion at a constant rate was chosen for the sake of simplicity of implementation and interpretation. The aim of this investigation was not to fully recreate the volumetric expansion that might take place in the



(a) Diagram of ETH triaxial device, after Trausch-Giudici (2004)



(b) Specimen before testing

Fig. 1. The experiments were performed using the triaxial devices of ETH Zurich.

field, where a constant inflow rate is unlikely. Given the lack of relevant data, the goal was to gain initial, quantifiable insight on the behaviour of liquefiable soil within a water inflow zone.

An effort was made to select volumetric expansion rates that lie within a realistic range. Initially, the maximum realisable volumetric strain rate in the field was calculated ($\dot{\epsilon}_{v,max}$). A liquefiable layer overlain by an impermeable layer was assumed, as a worst-case scenario (Fig. 2). Full liquefaction and a critical hydraulic gradient were considered within the liquefiable layer, leading to upwards water flow and to the formation of a water inflow zone beneath the impermeable layer. Conservatively assuming this zone to be of the height of the examined element, the maximum volumetric strain rate was calculated as:

$$\dot{\epsilon}_{v,max} = \frac{v_{D,max}}{h_0} = \frac{k \cdot i_{crit}}{h_0} = \frac{(G_s - 1)k}{(1 + e_0) h_0} \quad (1)$$

where $v_{D,max}$ is the maximum Darcy velocity, h_0 is the initial height of the element, k is the hydraulic conductivity, i_{crit} is the critical hydraulic gradient, G_s is the specific gravity of solids, and e_0 is the initial void ratio. Hydraulic conductivity change with the density of the liquefiable layer was taken to follow the formula of Kozeny-Carman (Kozeny, 1927; Carman, 1956), shown to be an accurate assumption for Hostun sand by Adamidis *et al.* (2020).

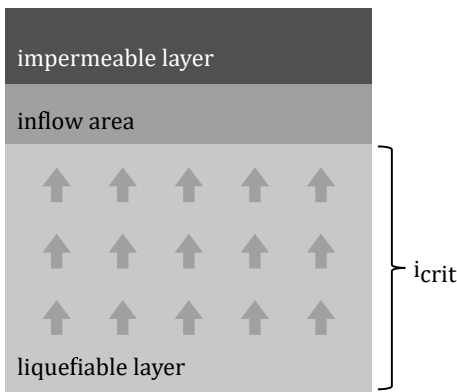


Fig. 2. Assumption for the calculation of $\dot{\epsilon}_{v,max}$: full liquefaction below the inflow zone and an impermeable layer above.

Using the above equation and assuming a typical frequency of loading for an earthquake, $f_{EQ} = 1 \text{ Hz}$, the maximum volumetric strain per cycle of loading was calculated. Since the utilised triaxial devices could only apply slow cyclic

loading, the maximum volumetric strain rate in the experiments ($\dot{\epsilon}_{v,max,exp}$) was chosen to produce the required maximum volumetric strain per cycle of loading:

$$\dot{\epsilon}_{v,max,exp} = \dot{\epsilon}_{v,max} \frac{f_{exp}}{f_{EQ}} \quad (2)$$

where f_{exp} represents the frequency of loading in the triaxial tests, kept at 0.005 Hz in these tests to maintain good load control when nearing liquefaction.

The maximum volumetric strain rate is meant to act as an upper limit. A more realistic, thicker water inflow zone (e.g., see the thickness of the inflow zone in the centrifuge experiments of Malvick *et al.* (2004), albeit for sloped ground) would lead to smaller volumetric strain rates. Moreover, a fully impermeable overlying layer is unlikely; a layer of low permeability would lead to volumetric expansion at a lower rate. Finally, a critical hydraulic gradient would not be immediately established within the liquefiable layer, further limiting the rate of volumetric expansion in proximity to the interface of the two layers. Following these considerations, rates of volumetric expansion significantly lower than the maximum were applied for the experiments presented here. Most experiments were performed using $\dot{\epsilon}_v = 5\% \dot{\epsilon}_{v,max}$, while an investigation for dense sand also included $\dot{\epsilon}_v = 1\% \dot{\epsilon}_{v,max}$ and $\dot{\epsilon}_v = 15\% \dot{\epsilon}_{v,max}$. When applied in the experimental setup, $\dot{\epsilon}_{v,max}$ was converted to $\dot{\epsilon}_{v,max,exp}$ following Eq. 2, so that the appropriate volumetric strain was imposed per loading cycle. The rates of volumetric expansion chosen are realistic when compared with the volumetric strains calculated by Malvick *et al.* (2008) in proximity to the interface of a liquefiable layer with an overlying layer of silt.

UNDRAINED CYCLIC RESISTANCE CURVES

Initially, the undrained response of the examined sand was established by conducting cyclic undrained triaxial experiments. An example of the results obtained from these tests is included in Fig. 3. As is typical of such experiments, an increased generation of ΔU was observed for the first cycle of loading, which decreased with subsequent cycles. As the specimen came closer to ‘full’ liquefaction ($R_u = \frac{\Delta U}{\sigma'_{v,0}} = 1$), the excess pore pressure and the maximum axial strain generated per cycle increased dramatically. Once the stress path came in proximity to the origin of the axes in the $q - p'$ space, characteristic ‘butterfly’ loops were produced. As expected, larger axial strains were observed in extension than in compression.

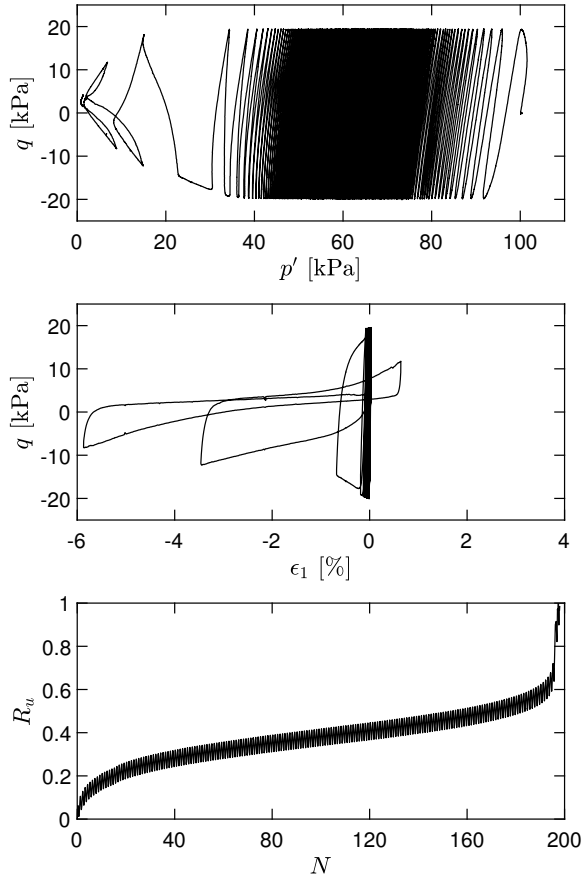
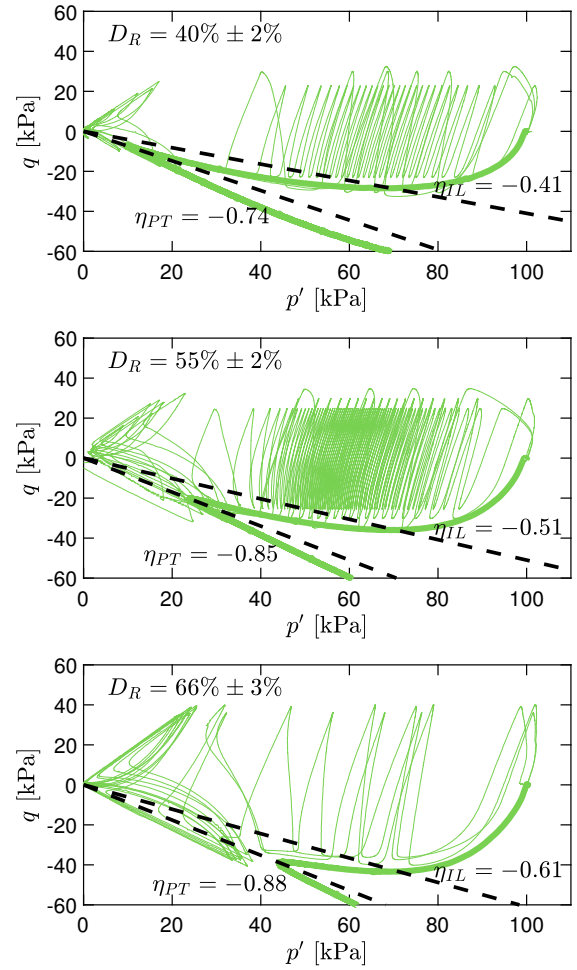


Fig. 3. Example of a cyclic undrained test ($D_R = 40\% \pm 2\%$, $\dot{\epsilon}_v = 0$).

In Fig. 4, cyclic undrained results are presented in the $q - p'$ space for three relative density ranges: $D_R = 40\% \pm 2\%$, $D_R = 55\% \pm 2\%$, and $D_R = 66\% \pm 3\%$. Overlain in thick lines are results from strain-controlled, monotonic undrained extension tests at the same relative density ranges. Based on these results, the stress ratio $\eta = q/p'$ corresponding to the state of instability (η_{IL}) and phase transformation (η_{PT}) for each examined relative density was calculated. Extension rather than compression tests are shown since the stress ratios corresponding to instability and phase transformation are lower in extension and are therefore reached first. The instability state corresponds to the point of the stress path beyond which 'flow liquefaction' can occur in a slope. More formally, it is defined as the point at which Hill's (1958) stability condition is no longer maintained. In undrained loading, it corresponds to the local extremum of deviatoric stress (Lade, 1992), as seen in Fig. 4. When the stress ratio of the cyclic undrained tests became larger than (η_{IL}), ΔU generation per cycle was increased. The phase transformation corresponds to the state that marks the transition from contractive to dilative behaviour (Ishihara *et al.*, 1975). In the undrained extension tests of Fig. 4, when the stress ratio of the cyclic undrained tests became larger than (η_{PT}), significant excess pore pressures were generated upon loading reversal, bringing the specimen in proximity to a condition of $R_u = 1$. Ishihara *et al.* (1975) considered the crossing of the phase transformation line as a criterion for the transformation from a solid to a liquefied state, hence the term 'phase transformation'.

Although the crossing of (η_{PT}) has been used as a criterion for the onset of liquefaction (Ishihara *et al.*, 1975), the most



— Monotonic undrained extension tests
— Cyclic undrained tests

Fig. 4. Instability (η_{IL}) and phase transformation (η_{PT}) lines in extension (dashed lines), defined from monotonic undrained extension tests.

common criteria are those proposed by Seed & Lee (1966). The first criterion requires ΔU equal to the initial p' , so that $R_u = 100\%$. The second criterion requires double amplitude axial strain of more than 5%.

The results from the series of cyclic undrained experiments are compiled in Fig. 5, presented as cyclic resistance curves. The abscissa shows the number of loading cycles (N) in logarithmic scale, while the ordinate depicts the Cyclic Stress Ratio (CSR). CSR is defined as the ratio of the amplitude of cyclic shearing (τ_{cyc}) to the initial vertical effective stress ($\sigma'_{v,0}$), corresponding in the isotropically consolidated triaxial tests examined here to the ratio of half the amplitude of cyclic deviatoric stress ($q_{max}/2$) to the initial mean effective stress p'_0 :

$$CSR = \frac{\tau_{cyc}}{\sigma'_{v,0}} = \frac{q_{max}}{2p'_0} \quad (3)$$

The points included in Fig. 5 correspond to the three criteria for the onset of liquefaction described above: double amplitude axial strain $\epsilon_{1,DA} = 5\%$, excess pore water pressure ratio $R_u = 100\%$, and crossing of the phase transformation line in extension (η_{PT_e}). The three criteria were generally in good agreement, apart from the case of dense sand at low CSR . There, the criteria of $R_u = 100\%$ and η_{PT_e} gave similar values,

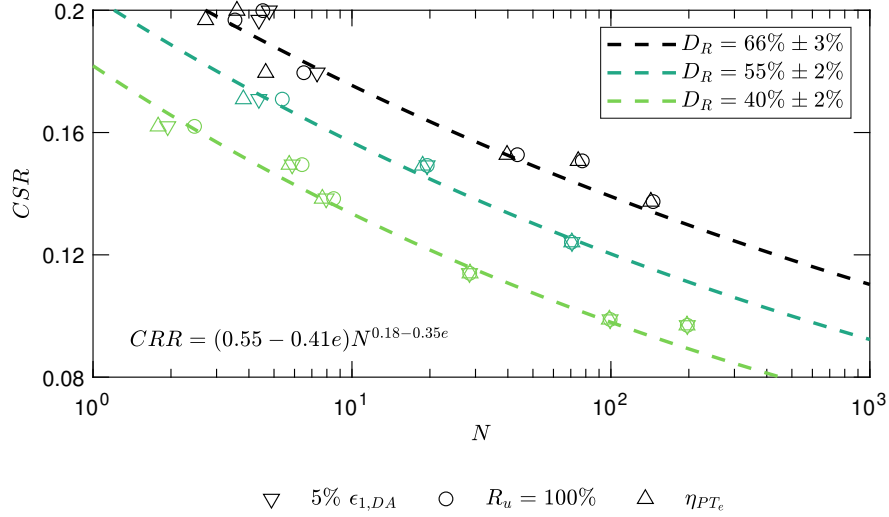


Fig. 5. Undrained cyclic resistance curves. The onset of liquefaction is marked using three criteria: (a) double amplitude axial strain of 5%, (b) excess pore water pressure ratio of 100%, and (c) crossing of the phase transformation line in extension. The dashed lines correspond to Eq. 4.

while the criterion of $\epsilon_{1,DA} = 5\%$ was not met at the end of the experiments, requiring further cycles of loading than those applied. This response is not uncommon for dense, dilative sands, which exhibit cyclic mobility. In such cases, axial strain is not generated in a sudden and extreme manner but rather develops incrementally, even after the criterion of $R_u = 100\%$ has been met for the first time. In fact, $R_u = 100\%$ is only attained temporarily within loading cycles, as dilation leads to transient increases in effective stress, which in turn prevent the quick accumulation of large strains. It is worth noting that due to the logarithmic abscissa of Fig. 5, differences between criteria appear exaggerated for numbers of cycles below 10, though in reality they are not that significant.

Figure 5 includes results for three density ranges: $D_R = 40\% \pm 2\%$, $D_R = 55\% \pm 2\%$, and $D_R = 66\% \pm 3\%$. As density increases, more loading cycles are required to cause liquefaction for the same CSR. The CSR required to cause liquefaction for a given number of loading cycles N is called here the Cyclic Resistance Ratio (CRR) for this number of cycles. Starting with the experimental points of Fig. 5, Eq. 4 is proposed, which gives (CRR) as a function of the number of loading cycles (N) and the specimen's void ratio (e):

$$CRR = (0.55 - 0.41e)N^{0.18-0.35e} \quad (4)$$

As seen in the figure, this expression provides a good fit for the range of relative densities and loading cycles examined experimentally.

The cyclic triaxial experiments included in Fig. 5 are listed in Table 2, along with their initial properties and the results regarding the number of cycles to liquefaction, with the three criteria considered.

WATER INFLOW CYCLIC RESISTANCE CURVES

Having established the cyclic resistance curves under undrained conditions, the cyclic triaxial experiments were repeated, this time under a constant water inflow condition, which led to constant rates of volumetric expansion. The selected rates of volumetric expansion were fractions of the maximum realisable rate of $\dot{\epsilon}_{v,max}$ of Eq. 1, so as to be more realistic, as previously explained.

Even a small rate of volumetric expansion can have a dramatic impact on cyclic resistance. In Fig. 6, a cyclic triaxial experiment on loose sand with a volumetric expansion rate of $\dot{\epsilon}_v = 5\%\dot{\epsilon}_{v,max}$ is overlain on the experiment of Fig. 3, which is of a specimen of the same density subjected to cyclic loading with the same CSR but under undrained conditions. Although in the experiment with water inflow the rate of volumetric expansion was very low (the void ratio change per cycle is $de/cycle = 0.0008$), a striking drop was recorded in the number of cycles required to cause liquefaction. The undrained prediction in this case was far from conservative.

For a specimen undergoing volumetric expansion, the number of cycles to liquefaction cannot be anticipated using undrained resistance curves for an 'equivalent' reduced density. When the specimen with the inflow condition of Fig. 6 reached liquefaction, its void ratio had increased by only 0.007 compared to its initial value. An undrained prediction using Eq. 4 for the final, increased void ratio of the specimen would significantly overestimate its cyclic resistance.

Results for cyclic resistance curves under a volumetric expansion rate of $\dot{\epsilon}_v = 5\%\dot{\epsilon}_{v,max}$ are presented in Fig. 7. A dramatic drop in cyclic resistance was caused by the imposed expansion throughout the range of densities examined. For large values of CSR, where liquefaction under undrained conditions was attained within few cycles, the differences were small. However, as CSR reduced, the undrained cyclic resistance curve deviated further from the one under an inflow condition. Importantly, liquefaction was always reached within less than 20 cycles under inflow, even for very low levels of CSR, where no liquefaction was attained after 1000 undrained cycles. Overall, the 'safe' area found below the undrained cyclic resistance curves of Fig. 7 (corresponding to loading that does not lead to liquefaction) was significantly diminished under the inflow condition.

The triaxial experiments with an inflow condition included in Fig. 7 are summarised in Table 2, which includes their initial properties and the number of cycles required to reach liquefaction with the three criteria also considered for the cyclic undrained tests.

Table 2. List of cyclic triaxial experiments performed and main results.

Test ID	e_0 (—)	D_R (%)	p'_0 (kPa)	CSR (—)	$\frac{\epsilon_{v,max}}{cycle}$ (%)	$\frac{\dot{\epsilon}_v}{\epsilon_{v,max}}$ (%)	$\frac{\epsilon_v}{cycle}$ (%)	$\frac{de}{cycle}$ (—)	N_{ϵ_1} (—)	N_{R_u} (—)	N_{PT_e} (—)
ICT40/100/19/0	0.894	41	100	0.10	-0.94	0	0	0	197.3	197.3	196.7
ICT40/100/20/0	0.900	39	100	0.10	-0.96	0	0	0	99.3	99.3	98.7
ICT40/100/23/0	0.905	38	100	0.11	-0.97	0	0	0	28.4	28.5	28.6
ICT40/100/28/0	0.891	42	100	0.14	-0.95	0	0	0	8.0	8.1	7.7
ICT40/100/30/0	0.899	40	100	0.15	-0.97	0	0	0	5.9	6.4	5.7
ICT40/100/33/0	0.901	39	100	0.16	-0.97	0	0	0	1.9	2.5	1.8
ICT40/100/12/5	0.902	39	100	0.06	-0.97	5	-0.05	0.0009	-	11.8	11.7
ICT40/100/20/5	0.892	41	100	0.10	-0.94	5	-0.04	0.0008	9.5	9.5	8.7
ICT40/100/22/5	0.893	41	100	0.11	-0.97	5	-0.05	0.0009	6.7	7.0	6.7
ICT40/100/25/5	0.893	41	100	0.13	-0.97	5	-0.04	0.0008	5.0	5.1	4.8
ICT55/100/25/0	0.835	57	100	0.12	-0.83	0	0	0	70.7	70.4	70.6
ICT55/100/30/0	0.849	53	100	0.15	-0.85	0	0	0	19.5	19.5	18.8
ICT55/100/34/0	0.844	54	100	0.17	-0.84	0	0	0	4.4	5.4	3.8
ICT55/100/15/5	0.839	56	100	0.07	-0.82	5	-0.04	0.0007	-	15.5	14.8
ICT55/100/25/5	0.846	54	100	0.13	-0.84	5	-0.04	0.0007	-	7.5	6.7
ICT55/100/30/5	0.847	53	100	0.15	-0.85	5	-0.04	0.0007	3.7	4.5	3.7
ICT65/100/28/0	0.794	68	100	0.14	-0.73	0	0	0	-	144.5	142.7
ICT65/100/30/0	0.804	65	99	0.15	-0.60	0	0	0	-	43.5	39.7
ICT65/100/30/0	0.805	65	100	0.15	-0.75	0	0	0	-	77.5	74.8
ICT65/100/36/0	0.793	68	100	0.18	-0.73	0	0	0	7.3	6.5	4.6
ICT65/100/39/0	0.802	65	99	0.20	-0.75	0	0	0	4.4	3.5	2.7
ICT65/100/40/0	0.811	63	100	0.20	-0.77	0	0	0	4.8	4.5	3.6
ICT65/100/10/1	0.794	68	100	0.05	-0.74	1	-0.01	0.0001	-	68.1	64.7
ICT65/100/13/1	0.788	69	99	0.07	-0.72	1	-0.01	0.0001	-	66.5	61.7
ICT65/100/20/1	0.790	68	100	0.10	-0.73	1	-0.01	0.0001	-	40.5	37.8
ICT65/100/28/1	0.809	64	99	0.14	-0.76	1	-0.01	0.0001	-	26.1	23.7
ICT65/100/10/5	0.799	66	100	0.05	-0.74	5	-0.04	0.0007	-	16.4	15.7
ICT65/100/20/5	0.805	65	100	0.10	-0.75	5	-0.04	0.0007	11.5	11.1	9.8
ICT65/100/30/5	0.800	66	100	0.15	-0.75	5	-0.03	0.0006	5.4	5.4	4.6
ICT65/100/15/15	0.790	68	100	0.07	-0.73	15	-0.10	0.0019	6.5	5.1	4.6
ICT65/100/20/15	0.787	69	101	0.10	-0.72	15	-0.10	0.0018	-	5.5	4.7
ICT65/100/25/15	0.797	67	100	0.13	-0.74	15	-0.10	0.0018	5.5	4.5	3.6
ICT65/100/30/15	0.790	68	100	0.15	-0.72	15	-0.08	0.0014	3.5	3.5	2.7

Test ID includes: (1) type of consolidation: I for isotropic, (2) type of experiment: CT for cyclic triaxial, (3) targeted relative density (%), (4) targeted initial mean effective stress (kPa), (5) amplitude of cyclic deviatoric stress (kPa), and (6) targeted ratio of $\dot{\epsilon}_v/\dot{\epsilon}_{v,max}$ (%).

e_0 : Void ratio after consolidation and before cyclic loading.

N_{ϵ_1} : Number of cycles for double amplitude of axial strain of 5%.

N_{R_u} : Number of cycles for $R_u = 100\%$.

N_{PT_e} : Number of cycles for crossing of the phase transformation line in extension.

SIMPLIFIED PREDICTION

The results of Fig. 7 demonstrate the sensitivity of cyclic resistance curves to drainage conditions, with a small rate of water inflow resulting in a significant drop in the number of cycles required for liquefaction. However, each cyclic resistance curve under a water inflow rate involves multiple non-standard triaxial experiments, which might be difficult to reproduce in practice. Moreover, Fig. 7 includes results for only one fraction of the maximum realisable volumetric expansion rate: $\dot{\epsilon}_v = 5\%\dot{\epsilon}_{v,max}$. Cyclic resistance curves for multiple rates of water inflow are necessary before results can be generalised, so as to be taken into account in liquefaction susceptibility assessments. In order to tackle these issues, a simplified methodology is proposed, which can adequately predict cyclic resistance curves under any constant volumetric expansion rate. As input, the methodology requires results from standardised testing: (a) the cyclic undrained experiments required to produce undrained cyclic resistance curves, and (b) an isotropic unloading curve for the examined material. In

order to be used as a liquefaction onset criterion, the phase transformation line in extension should also be known. It could either be inferred from cyclic undrained experiments, or determined through monotonic extension tests, as shown in Fig. 4.

At the core of the proposed methodology is the assumption that the decrease in mean effective stress for specimens subjected to volumetric expansion is due to: (a) isotropic unloading as a result of volumetric expansion, and (b) excess pore pressure generation as a result of cyclic shearing.

Isotropic Unloading

In order to quantify the effects of unloading, triaxial experiments were performed to establish the incremental bulk modulus under isotropic unloading. Results from three experiments are shown in Fig. 8, spanning the range of relative densities of interest. Following the form of the expression proposed by Pestana & Whittle (1995), the incremental bulk

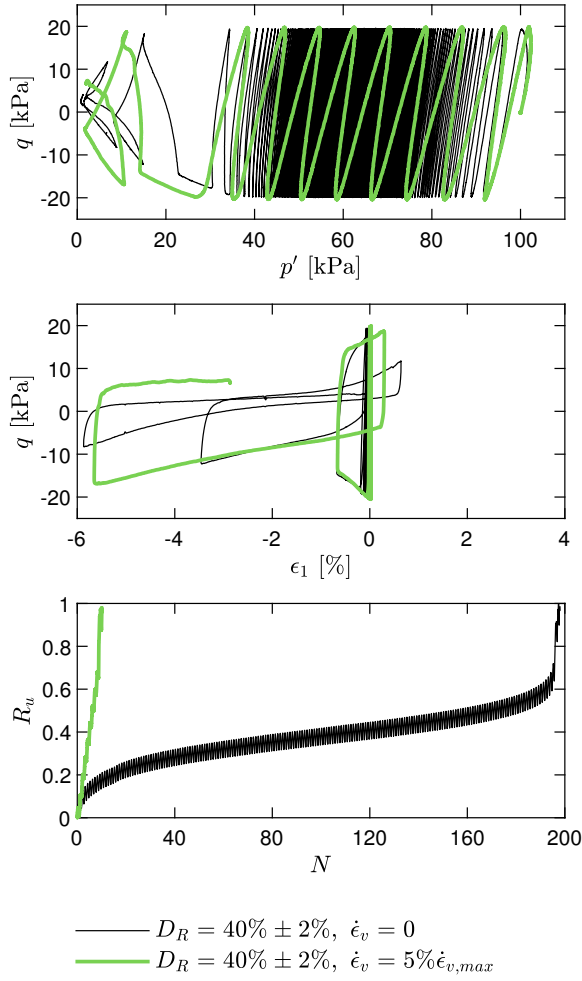


Fig. 6. Example of a partially drained cyclic test with constant rate of volumetric expansion, overlain on an undrained cyclic test of the same relative density and the same CSR .

modulus in isotropic unloading was described as follows:

$$\frac{K}{p_a} = C \cdot f_1(e) \cdot f_2\left(\frac{p'}{p_a}\right) \quad (5)$$

where K is the incremental bulk modulus in isotropic unloading, p_a the atmospheric pressure, used as an arbitrary reference stress, C a constant, $f_1(e)$ a function of void ratio e , and $f_2\left(\frac{p'}{p_a}\right)$ a function of normalised mean effective stress p' .

Functions $f_1(e)$ and $f_2(p'/p_a)$ are typically required to satisfy the following criteria: $\frac{\partial K}{\partial e}\big|_{p'} < 0$ and $\frac{\partial K}{\partial p'}\big|_e > 0$, so that the incremental bulk modulus decreases with increasing void ratio and increases with increasing stress. Function $f_2(p'/p_a)$ typically takes the form of a power law in expressions of stiffness, which satisfies the criterion mentioned above. A power law was also adopted here: $f_2(p'/p_a) = (p'/p_a)^B$. Figure 8 presents results for the normalised incremental bulk modulus in unloading as a function of normalised p' , both in logarithmic scale. A single slope can be used to fit the results, which corresponds to the exponent B ; here $B = 0.65$. Function $f_1(e)$ was defined as: $f_1(e) = 1/e^2$, a form which satisfies the criterion presented above and provides a good fit of the experimental results across the examined densities. The dashed line included in Fig. 8, which corresponds to the expression adopted for the incremental bulk modulus under

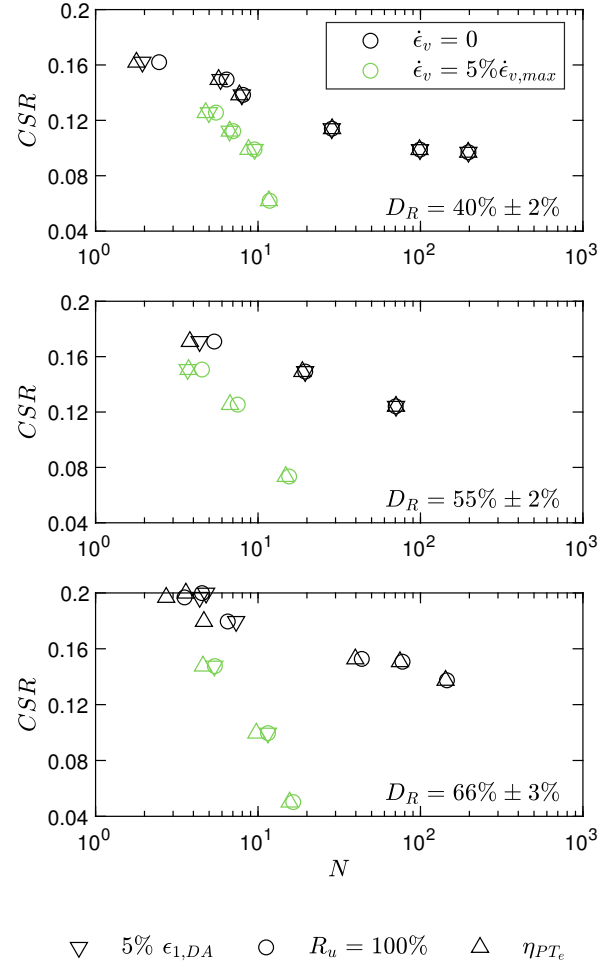


Fig. 7. Cyclic resistance results under undrained conditions ($\dot{\epsilon}_v = 0$) and under a constant rate of volumetric expansion ($\dot{\epsilon}_v = 5\%\dot{\epsilon}_{v,max}$)

isotropic unloading, is the following:

$$\frac{K}{p_a} = \frac{C}{e^2} \left(\frac{p'}{p_a}\right)^B \quad (6)$$

with $C = 180$ and $B = 0.65$.

This expression, which refers to the incremental bulk modulus in isotropic unloading, can be integrated over an unloading path from initial state (p'_0, e_0) to state (p', e) , to produce an unloading curve, expressed either with e as a function of p' (Eq. 7) or vice versa (Eq. 8).

$$e = \left[\frac{1}{e_0} + \frac{p_a^{B-1}(1+e_0)}{C(1-B)} \left(p'^{1-B} - p_0'^{1-B} \right) \right]^{-1} \quad (7)$$

$$p' = \left[\left(\frac{1}{e} - \frac{1}{e_0} \right) \frac{C(1-B)}{1+e_0} p_a^{1-B} + p_0'^{1-B} \right]^{\frac{1}{1-B}} \quad (8)$$

In Fig. 9, Eq. 7 is plotted as a dashed line over the experimental results. The proposed equation is shown to adequately predict the experimentally recorded unloading behaviour, over the range of relative densities of interest. In the proposed simplified methodology, the volumetric expansion rate is known, thus Eq. 8 can be used to calculate the reduction in p' caused by volumetric expansion.

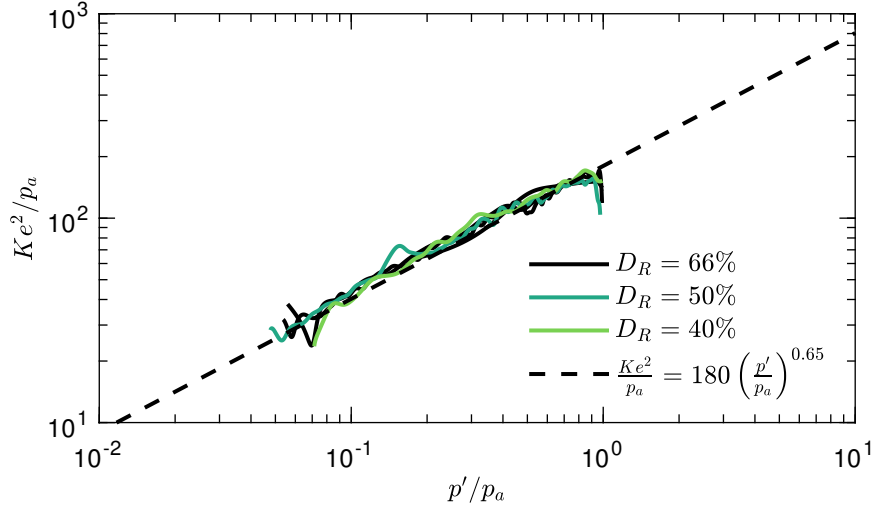


Fig. 8. Calculation of the incremental bulk modulus in unloading, over the range of relative densities of interest.

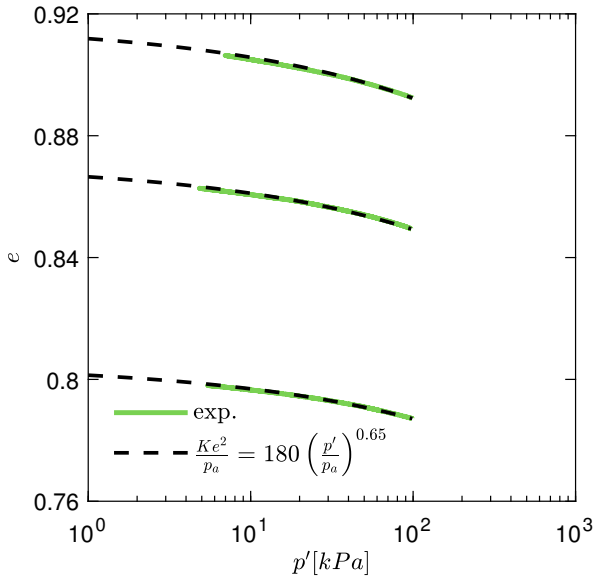


Fig. 9. Comparison of the experimentally measured isotropic unloading to that estimated using Eq. 7.

Undrained shearing

Having quantified the decrease in p' due to volumetric expansion, the potential further decrease as a result of cyclic shearing was addressed. At a first instance, this can be done by assuming superposition of undrained shearing and volumetric expansion. This assumption is simplistic but easy to implement, as it requires only the standardised experiments performed for undrained cyclic resistance curves as input. Whether it is sufficiently accurate is examined below.

Figure 10 presents all the experimental data on the undrained generation of excess pore pressure ratio R_u in function of the normalised number of stress-controlled loading cycles $n = \frac{N}{N_{ult}}$, where N_{ult} is the ultimate number of cycles required to cause liquefaction under undrained shearing. The criterion chosen for the determination of N_{ult} was the stress path crossing the phase transformation line in extension (η_{PTe}), to ensure consistency with its later use by the proposed

simplified methodology. No significant change would occur if the $R_u = 100\%$ criterion was chosen (Fig. 5). The points plotted depict R_u at instances of zero deviatoric stress. The experimental points correspond to a range of relative densities and amplitudes of cyclic loading (see Table 2) but within the normalised axes of Fig. 10 they form a narrow band that can be approximately described by an expression relating R_u to n . Many alternative such expressions exist in literature for stress-controlled cycles, either estimating R_u in function of n (e.g., Lee & Albaisa, 1974; ?; Baziar *et al.*, 2011), or estimating incremental increases in excess pore water pressure ΔU with subsequent loading cycles (e.g., Konstadinou & Georgiannou, 2014). Here, a set of expressions is proposed to fit the experimental data:

$$R_u = \frac{1}{b} n^a, \quad n \leq n_r \quad (9)$$

$$R_u = 1 - \frac{1}{d} (1 - n)^c, \quad n > n_r \quad (10)$$

The first expression (Eq. 9) is a power law that applies until the inflection point of the curve formed by the data points of Fig. 10. The inflection point $(n_r, R_{u,r})$ is taken as a reference which gives the first two input parameters required: n_r and $R_{u,r}$. The third input parameter, a , is the exponent of the power law, which controls curvature. Parameter b is calculated from the input parameters to ensure that the produced curve passes through the reference point (Eq. 11). Beyond the reference point ($n > n_r$), Eq. 10 applies. This expression is another power law, passing through the reference point with the same slope as Eq. 9, while also giving $R_u = 1$ at $n = 1$. Equation 10 does not require any additional input parameters. Parameters c and d are calculated from the input parameters as shown in Eqs. 12 and 13, respectively.

$$b = \frac{n_r^a}{R_{u,r}} \quad (11)$$

$$c = \frac{a n_r^{a-1} (1 - n_r)}{b - n_r^a} \quad (12)$$

$$d = \frac{b (1 - n_r)^c}{b - n_r^a} \quad (13)$$

For the experiments examined herein, the input parameters were selected as: $n_r = 0.5$, $R_{u,r} = 0.4$, and $a = 0.3$. The

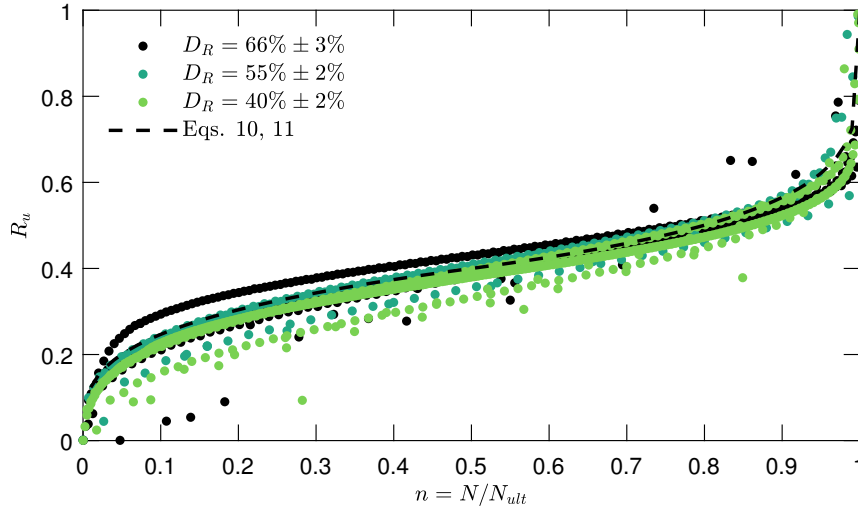


Fig. 10. Undrained excess pore water pressure generation. The experimental points correspond to instances of zero deviatoric stress. The criterion of phase transformation line crossing was used to determine N_{ult} . The proposed expression for R_u (dashed line), is given in Eqs. 9 and 10.

resulting curve is a good fit to the experimental data, as shown in Fig. 10. When using such an expression, the value of N_{ult} can be specified from the appropriate undrained cyclic resistance curve, for instance as expressed in Eq. 4.

For the sake of completeness, it should be noted that alternative approaches exist for the estimation of excess pore water pressure. A strong case for performing cyclic loading with controlled strain rather than stress was presented by Dobry *et al.* (1982). More recently, excess pore water pressure generation has been linked to the amount of dissipated energy, following the energy-based method first introduced by Nemat-Nasser & Shokoh (1979). However, in the context of developing a simplified methodology for cyclic resistance curves, expressions that describe R_u in function of stress-controlled loading cycles (N) are ideal, since cyclic resistance curves are also functions of N . In addition, this approach does not require experiments beyond those for the undrained cyclic resistance curves. Indeed, Eqs. 9 and 10 were derived using only the experiments performed to generate the undrained cyclic resistance curves of Fig. 5.

Onset of liquefaction

The proposed simplified methodology assumes a specimen's response during cyclic loading under constant volumetric expansion can be interpreted as a superposition of unloading and cyclic shearing. Following this hypothesis, in specimens subjected to cyclic loading under a very low CSR , the contribution of cyclic shearing to the reduction of p' should be minimal. These are specimens for which hundreds of loading cycles would be required to reach liquefaction under undrained conditions. Instead, it should be isotropic unloading due to volumetric expansion that primarily drives the reduction in p' and the stress path should follow more closely that of isotropic unloading. As CSR increases and the number of undrained cycles to liquefaction drops (Eq. 4), the simplified methodology assumes that cyclic shearing has a more significant contribution in the reduction of effective stress. As a result, the stress path should deviate more from that of isotropic unloading, with p' reducing faster.

In Fig. 11, the change in void ratio (δe) relative to p' is shown for three specimens of each density range examined. Isotropic unloading lines (Eqs. 7 and 8) are superposed on the

graphs. Specimens loaded under a very low CSR closely follow the isotropic unloading line, as the proposed methodology assumes. For specimens loaded under a higher CSR , paths deviate to the left of the isotropic unloading line, as assumed by the methodology. Before examining whether superposition of isotropic unloading and undrained shearing is sufficient for a reliable prediction of liquefaction, a criterion for its onset must be chosen. To provide consistency with undrained cyclic resistance curves, the criterion of double amplitude axial strain of more than 5% was not considered, as it was observed to give too high numbers of cycles to reach liquefaction for undrained loading of dense specimens.

For the experiments under constant volumetric expansion presented in Fig. 11, the criterion of crossing the phase transformation line in extension (points marked with a triangle) was preferred to the $R_u = 100\%$ criterion for the identification of liquefaction triggering. The phase transformation criterion was satisfied during a large reduction in effective stress that brought p' to very low values, albeit not low enough to satisfy the $R_u = 100\%$ criterion. Especially for dense specimens, where dilation was more prominent, several additional cycles were required for the $R_u = 100\%$ criterion to be met, even though specimens lost most of their shear strength once the phase transformation was crossed. Considering the low number of cycles required to reach liquefaction under volumetric expansion, the addition of extra cycles to satisfy $R_u = 100\%$ can lead to values that are not representative of when a specimen loses most of its initial effective stress. As a result, the phase transformation criterion was chosen for the proposed methodology.

The phase transformation lines used are shown in Fig. 4, determined from undrained extension tests. Although these tests are easier to interpret, one could alternatively infer phase transformation lines from the cyclic tests of the undrained cyclic resistance curves, limiting the total number of experiments. For a comparison, see Fig. 4, where undrained extension tests are superposed on cyclic undrained tests. The phase transformation lines derived from undrained testing perform well as liquefaction criteria for the volumetric expansion tests of Fig. 11. Of course, attention is required in using values that correspond to the appropriate density.

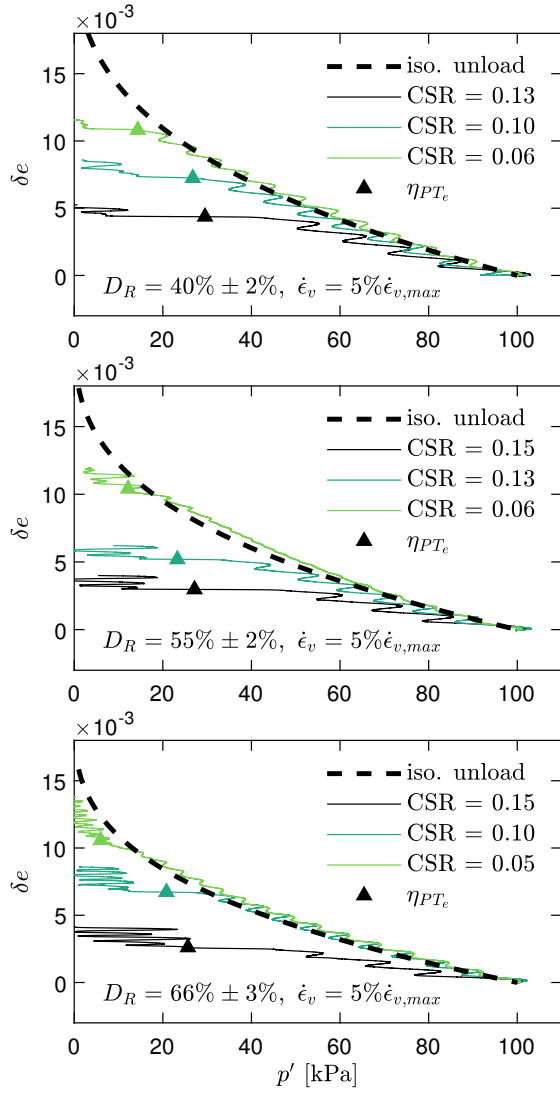


Fig. 11. Change in voids ratio δe with decreasing mean effective stress p' for cyclic loading experiments under a constant volumetric expansion rate $\dot{\epsilon}_v = 5\% \dot{\epsilon}_{v,max}$. The isotropic unloading curve is superposed and the instants when the phase transformation line in extension (η_{PT_e}) is crossed are highlighted.

Estimation of cyclic resistance

With relations in place to quantify the effects of unloading and shearing, and to assess liquefaction triggering, a methodology to evaluate cyclic resistance under constant volumetric expansion was fully developed. The process is outlined schematically in Fig. 12.

The input parameters for this methodology include:

- a the Cyclic Stress Ratio (CSR)
- b the loading frequency (f)
- c the constant volumetric expansion rate ($\dot{\epsilon}_v$)
- d the initial state of the element (p'_0, e_0)

In order to make evaluations, the following results from standardised element tests are required:

- a the undrained cyclic resistance curve (Eq. 4), generated using standardised cyclic undrained tests
- b the isotropic unloading curve (Eq. 8), generated using drained isotropic unloading tests
- c the phase transformation line in extension (η_{PT_e}), determined through monotonic extension tests or inferred

from the cyclic undrained tests of the undrained cyclic resistance curve (Fig. 4).

Firstly, the contribution of isotropic unloading on the reduction of p' is estimated. The imposed volumetric expansion rate $\dot{\epsilon}_v$ corresponds to volumetric strain as a function of time (expansion is taken as negative):

$$\epsilon_v(t) = \dot{\epsilon}_v \cdot t \quad (14)$$

which in turn corresponds to change in void ratio:

$$\delta e(t) = -\epsilon_v(t)/(1 + e_0) \quad (15)$$

and gives:

$$e(t) = e_0 + \delta e(t) \quad (16)$$

Using this updated void ratio and the initial state of the element (p'_0, e_0), the reduction in p' due to isotropic unloading can be calculated through Eq. 8 as a function of time:

$$\delta p'_{unl}(t) = \left[\left(\frac{1}{e(t)} - \frac{1}{e_0} \right) \frac{C(1-B)}{1+e_0} p_a^{1-B} + p'^{1-B}_0 \right]^{\frac{1}{1-B}} - p'_0 \quad (17)$$

with $C = 180$ and $B = 0.65$ for Hostun sand.

Secondly, the contribution of shearing on the reduction of p' is examined. Using the imposed CSR and the current state (p'_0, e_0), the number of undrained cycles required to reach liquefaction (N_{ult}) is estimated from the undrained cyclic resistance curve. Here, from Eq. 4:

$$N_{ult} = \left(\frac{CSR}{0.55 - 0.41e_0} \right)^{1/(0.18 - 0.35e_0)} \quad (18)$$

Using N_{ult} , the generation of excess pore water pressure ratio is expressed in function of normalised undrained loading cycles. Further, by incorporating the loading frequency, excess pore pressure ratio can be expressed as a function of time. For Hostun sand, Eqs. 9 and 10 give:

$$R_u(t) = \frac{1}{b} \left(\frac{t \cdot f}{N_{ult}} \right)^a, \quad \frac{t \cdot f}{N_{ult}} \leq n_r \quad (19)$$

$$R_u(t) = 1 - \frac{1}{d} \left(1 - \frac{t \cdot f}{N_{ult}} \right)^c, \quad \frac{t \cdot f}{N_{ult}} > n_r \quad (20)$$

with $n_r = 0.5$, $a = 0.3$, and b, c, d defined from Eqs. 11, 12, and 13, respectively, using $R_{u,r} = 0.4$. Also considering the initial state (p'_0, e_0), the reduction in p' due to shearing is estimated as a function of time:

$$\delta p'_{shr}(t) = -p'_0 \cdot R_u(t) \quad (21)$$

The total reduction in p' in function of time is given by adding the reductions due to unloading and shearing:

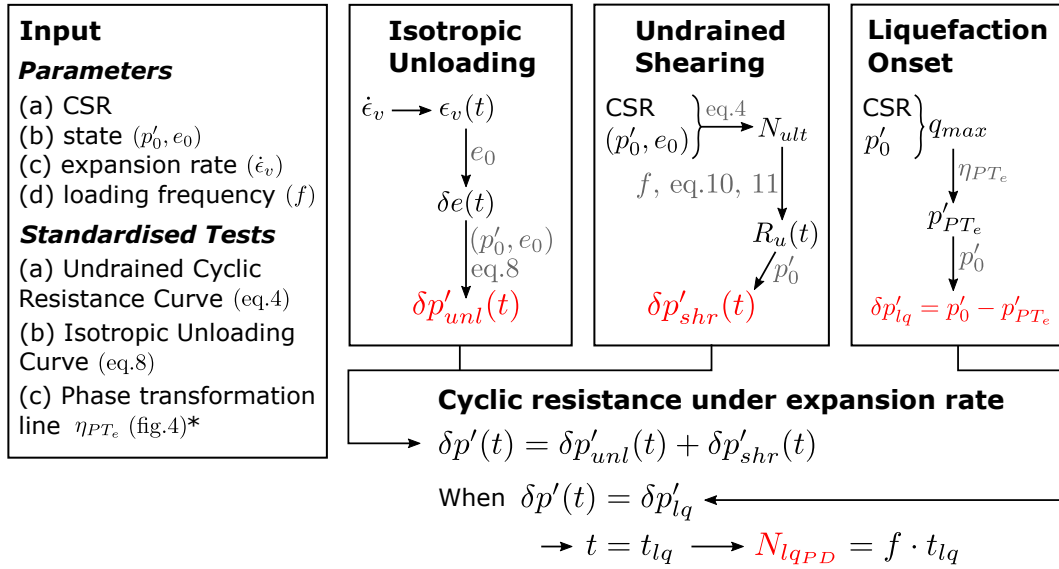
$$\delta p'(t) = \delta p'_{unl}(t) + \delta p'_{shr}(t) \quad (22)$$

In order to assess the $\delta p'$ that is sufficient to trigger liquefaction, a simplified assumption is made for the crossing of the phase transformation line in extension. Using the imposed CSR and the initial state (p'_0, e_0), the maximum deviatoric stress q_{max} is calculated, from the definition of CSR (eq. 3):

$$q_{max} = 2p'_0 \cdot CSR \quad (23)$$

The value of p' that gives a stress ratio equal to η_{PT_e} for the maximum deviatoric stress is then estimated:

$$p'_{PT_e} = q_{max}/\eta_{PT_e} \quad (24)$$



* η_{PT_e} could come from the experiments for the Undrained Cyclic Resistance Curve

Fig. 12. Outline of the simplified method proposed to evaluate cyclic resistance under a constant expansion rate.

Finally, using the initial state (p'_0, e_0), the required reduction in p' for liquefaction to be triggered can be evaluated:

$$\delta p'_{lq} = p'_0 - p'_{PT_e} \quad (25)$$

The time instant t_{lq} at which $\delta p'$ reaches $\delta p'_{lq}$ is when liquefaction is triggered:

$$\delta p'(t_{lq}) = \delta p'_{lq} \quad (26)$$

Time can be converted back to number of cycles using the loading frequency:

$$N_{lqPD} = f \cdot t_{lq} \quad (27)$$

Thus, the cyclic resistance to liquefaction for the requested CSR and volumetric expansion rate is estimated, given the loading frequency and the initial state.

Examples of the estimated reduction in mean effective stress $\delta p'(t)$ (Eq. 22) as the void ratio changes $\delta e(t)$ (Eq. 15) are shown in Fig. 13, for three cyclic loading cases of different density. The chosen cases correspond to the highest CSR experiments of Fig. 11, for which shearing has a more significant contribution and the superposition assumption is more severely tested. Both estimated and experimentally measured values are included in Fig. 13 for comparison. The points of liquefaction triggering are denoted with a triangle marker. Especially as the sand gets looser, the assumption of superposition of unloading with undrained shearing leads to more significant reduction in p' than that measured in experiments. Nevertheless, the overall comparison remains satisfactory. The trends of the experimental paths are captured adequately and the predicted points of liquefaction triggering are very close to the experimental ones.

Cyclic resistance curves

By applying the methodology proposed above for a range of CSR values, a full cyclic resistance curve under a constant volumetric expansion rate can be computed. In Fig. 14, evaluated cyclic resistance curves under an expansion rate of $\dot{\epsilon}_v = 5\% \dot{\epsilon}_{v,max}$ are shown. The produced curves compare very well to the experimental results. For high CSR, the curves under volumetric expansion approach the undrained

ones. This is because in this region shearing drives the reduction in p' , triggering liquefaction within few cycles. In this time, unloading due to expansion has not had a significant effect. However, as CSR reduces, the curves under volumetric expansion deviate significantly from the undrained ones. This happens because the contribution of shearing reduces, with unloading due to expansion driving the reduction in p' . It is worth noting that if such an expansion condition was realised in the field, the remarkably large area between the expansion curve and the undrained curve would correspond to false negative predictions for liquefaction assessments with current methodologies.

The proposed methodology is shown to perform well for a range of densities in Fig. 14. Its performance was also assessed for a range of volumetric expansion rates, for specimens on the higher density range. The higher density range was chosen to showcase how a volumetric expansion condition can lead to liquefaction a sand that might be considered safe under undrained conditions. Additional expansion rates of $\dot{\epsilon}_v = 1\% \dot{\epsilon}_{v,max}$ and $\dot{\epsilon}_v = 15\% \dot{\epsilon}_{v,max}$ were examined. The corresponding experiments are listed in Table 2 and the experimental results are presented in Fig. 15, along with the predictions of the proposed methodology. Once again, the predicted curves compare very favourably with the experimental results, giving confidence on the reliability of the method for a wide range of densities and volumetric expansion rates.

In Fig. 15, one can observe that even for the very small inflow rate of $\dot{\epsilon}_v = 1\% \dot{\epsilon}_{v,max}$, significant reductions in the number of cycles required for liquefaction can be recorded. These reductions are important even for relatively high values of CSR, which would be enough to trigger pore pressure generation and upwards water flow; thus realising conditions of localised volumetric expansion in the presence of an overlying lower permeability layer. For instance, for a relatively high CSR of 0.15, the number of cycles to trigger liquefaction drops from 47 under undrained conditions to 16 for $\dot{\epsilon}_v = 1\% \dot{\epsilon}_{v,max}$. Thus, a site with layered deposits deemed safe with current methodologies might actually liquefy.

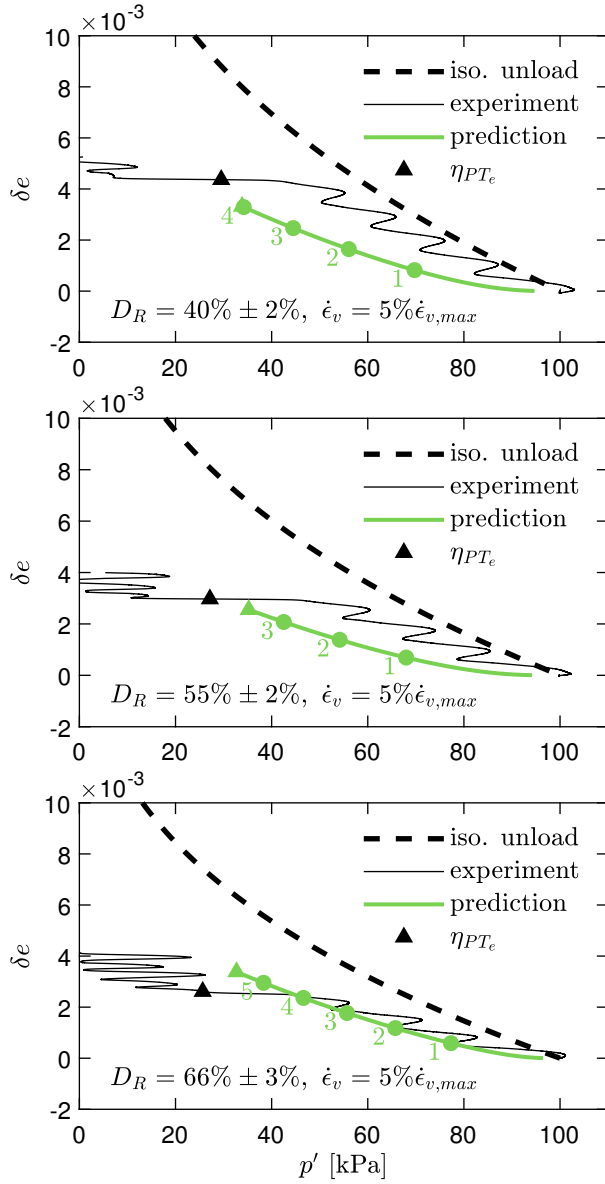


Fig. 13. Comparisons of paths in $\delta e - p'$ space: experimentally measured versus predicted with the proposed methodology. The triangular points denote when the onset of liquefaction, while the circular points on the predicted paths highlight the number of loading cycles.

CONCLUSIONS

Earthquake-induced liquefaction susceptibility assessments are often based on cyclic resistance curves, derived through undrained element tests. However, a growing body of evidence suggests that the undrained hypothesis is not realistic in the time-frame of an earthquake. Instead, partially drained conditions can be more appropriate. If a liquefiable layer is overlain by a lower permeability layer, upwards water flow during the earthquake can lead to localised, co-seismic pore volume increase in proximity to the interface of the layers. In such a case, assessments of liquefaction susceptibility on the basis of undrained cyclic resistance curves may lead to non-conservative predictions.

In this paper, the effects of localised volumetric expansion on cyclic resistance curves are quantified. A series of cyclic triaxial experiments is presented, performed either under undrained conditions or under conditions of a constant water inflow

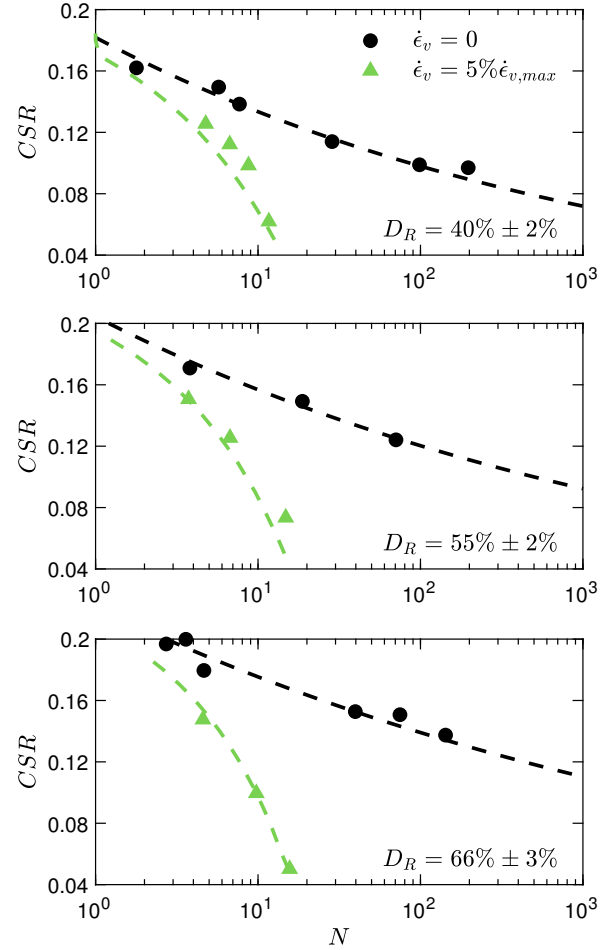


Fig. 14. Evaluation of the simplified methodology proposed for a range of densities. The circular points correspond to undrained experiments and the dashed line going through them is Eq. 4. The triangular points correspond to experiments under a constant expansion rate and the dashed line going through them is estimated following the proposed methodology.

rate. A constant inflow rate is assumed for the sake of simplicity, both regarding the experimental methodology and the interpretation of results.

Cyclic resistance curves for a range of densities and volumetric expansion rates are presented. Even small rates of volumetric expansion are shown to have a dramatic effect on cyclic resistance, significantly lowering the number of cycles required for liquefaction, as estimated under undrained conditions. Significant areas are enclosed between cyclic resistance curves under undrained conditions and under water inflow conditions. Should volumetric expansion due to water inflow be realised in the field, these areas would liquefy more easily than current liquefaction susceptibility assessments expect. If a low permeability non-liquefiable crust above a critical layer exists close to the surface, more severe liquefaction hazard than expected would exist, and such profiles could even be false-negatives under current prediction methodologies. If however, a liquefiable layer overlain by a lower permeability layer exists at depth, the outcome could be rapid liquefaction of the deep liquefiable layer, isolating the rest of the deposit and limiting the corresponding hazard by mitigating the effects of liquefaction close to the surface.

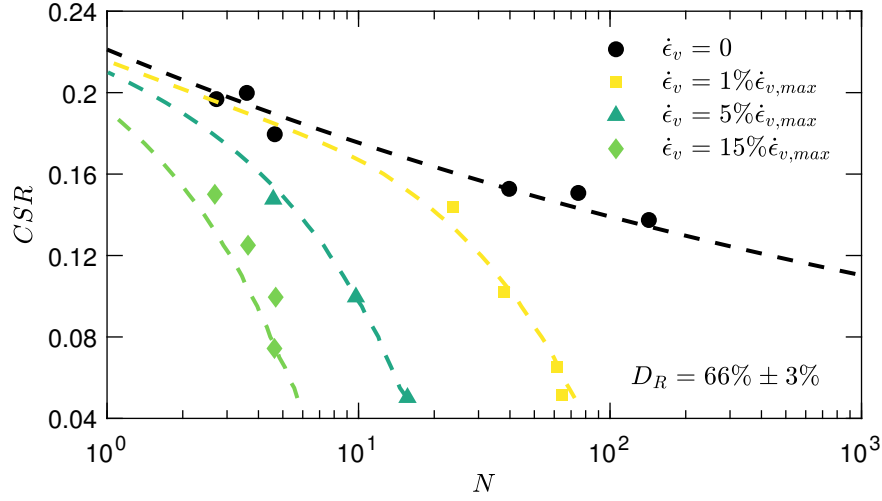


Fig. 15. Evaluation of the simplified methodology proposed for a range of volumetric expansion rates. The dashed lines are estimated following the proposed methodology.

The cyclic resistance curves presented herein were generated using a non-standard experimental procedure, controlling the water inflow rate during cyclic triaxial tests. Recognising that such tests might not be practical to reproduce, a simplified methodology is proposed, requiring as input only results derived from standardised element testing: (a) the undrained cyclic resistance curve, (b) a curve of isotropic unloading, and (c) the phase transformation line in extension, either determined from extension tests or inferred from the cyclic tests required to generate the undrained cyclic resistance curve. The methodology is based on the simplified assumption that reductions in mean effective stress can be attributed to a superposition of isotropic unloading due to volumetric expansion and excess pore pressure generation due to undrained shearing. Comparison with experimental results shows the proposed methodology to perform well throughout the examined range of densities and expansion rates for the examined, clean and poorly graded sand.

The presented results demonstrate the need for liquefaction susceptibility assessments to be updated in the case of deposits with layers of different permeability. In reality, variable rates of volumetric expansion might occur in proximity to the interface of such layers, which are not predicted by the methodology proposed here. However, the success of the proposed methodology in capturing experimental results indicates that the principle of superposition would be a reasonable assumption also for non-constant expansion rates. However, further research is needed to examine the limits of the superposition assumption, for instance under conditions of a static shear stress.

Finally, this research highlights significant aspects of soil response that must be captured by constitutive models used for liquefaction, in cases where partial drainage becomes important. Whereas currently the main focus is on capturing the effects of undrained shearing, it seems that the volumetric response is also of importance. The experimental results are included in the publication as a supplementary MATLAB data file.

ACKNOWLEDGEMENTS

Messrs R. Herzog, E. Bleiker, H. Buschor, and A. Kieper of the Institute for Geotechnical Engineering of ETH Zurich are

thankfully acknowledged for their technical assistance with the experimental setup. In addition, the authors thank Mr. S. Hekmati and Mss. N. Reckinger and C. Wirion of ETH Zurich for their help with experiments.

NOMENCLATURE

D_R	Relative Density
N_{ult}	Ultimate number of undrained loading cycles to liquefaction
$n = N/N_{ult}$	Normalised number of loading cycles
N_{lqPD}	Number of loading cycles to liquefaction under partial drainage
$d_{(x)}$	Particle size for which (x) % of the material is finer
e	Void ratio
e_0	Initial void ratio
f	Loading frequency
G_S	Specific gravity of solids
h_0	Initial height of element
i_{crit}	Critical hydraulic gradient
K	Incremental bulk modulus
k	Permeability
N	Number of loading cycles
p'	Mean effective stress
p'_0	Initial mean effective stress
p_a	Atmospheric pressure
q	Deviator stress
R_u	Excess pore water pressure ratio
v_D	Darcy velocity

ΔU	Excess pore water pressure
ϵ_1	Axial strain
ϵ_v	Volumetric strain
$\dot{\epsilon}_{v,max}$	Maximum volumetric strain rate for a liquefiable layer overlain by an impermeable layer
$\eta = q/p'$	Stress ratio
η_{IL}	Instability stress ratio
η'_{PT_e}	Phase transformation in extension stress ratio
ϕ_{crit}	Critical state friction angle
σ'_v	Vertical effective stress
τ	Shear stress
CPT	Cone Penetration Test
CRR	Cyclic Resistance Ratio
CSR	Cyclic Stress Ratio
SPT	Standard Penetration Test

REFERENCES

- Adamidis, O., Alber, S. & Anastasopoulos, I. (2020). Assessment of three-dimensional printing of granular media for geotechnical applications. *Geotechnical Testing Journal* **43**, No. 3, doi:10.1520/GTJ20180259.
- Adamidis, O. & Madabhushi, S. P. G. (2018a). Deformation mechanisms under shallow foundations on liquefiable layers of varying thickness. *Géotechnique* **68**, No. 7, 602–613, doi:10.1680/jgeot.17.P067.
- Adamidis, O. & Madabhushi, S. P. G. (2018b). Experimental investigation of drainage during earthquake-induced liquefaction. *Géotechnique* **68**, No. 8, 655–665, doi:10.1680/jgeot.16.P090.
- Andrianopoulos, K. I., Papadimitriou, A. G. & Bouckovalas, G. D. (2010). Bounding surface plasticity model for the seismic liquefaction analysis of geostructures. *Soil Dynamics and Earthquake Engineering* **30**, No. 10, 895–911, doi:10.1016/j.soildyn.2010.04.001.
- ASTM D4253-16e1 (2016). Standard Test Methods for Maximum Index Density and Unit Weight of Soils Using a Vibratory Table. *Technical report*, doi:10.1520/D4253-16E01.
- ASTM D4254-16 (2016). Standard Test Methods for Minimum Index Density and Unit Weight of Soils and Calculation of Relative Density. *Technical report*, doi:10.1520/D4254-16.
- ASTM D5311/D5311M-13 (2013). Standard Test Method for Load Controlled Cyclic Triaxial Strength of Soil. *Technical report*, doi:10.1520/D5311.
- Baziar, M. H., Shahnazari, H. & Sharafi, H. (2011). A laboratory study on the pore pressure generation model for Firouzkooh silty sands using hollow torsional test. *International Journal of Civil Engineering* **9**, No. 2, 126–134.
- Been, K. & Jefferies, M. G. (1985). A state parameter for sands. *Géotechnique* **35**, No. 2, 99–112, doi:10.1680/geot.1985.35.2.99, arXiv:1011.1669v3.
- Berrill, J. & Davis, R. (1985). Energy Dissipation and Seismic Liquefaction of Sands: Revised Model. *Soils and Foundations* **25**, No. 2, 106–118, doi:10.3208/sandf1972.25.2.106.
- Boulanger, R. & Ziotopoulou, K. (2013). Formulation of a sand plasticity plane-strain model for earthquake engineering applications. *Soil Dynamics and Earthquake Engineering* **53**, 254–267, doi:10.1016/j.soildyn.2013.07.006.
- Boulanger, R. W. & Idriss, I. M. (2014). CPT and SPT based liquefaction triggering procedures. *Center for Geotechnical Modeling UCD/CGM-14/01*, No. April, 134.
- Boulanger, R. W. & Idriss, I. M. (2016). CPT-Based Liquefaction Triggering Procedure. *Journal of Geotechnical and Geoenvironmental Engineering* **142**, No. 2, 04015065, doi:10.1061/(asce)gt.1943-5606.0001388.
- Carman, P. C. (1956). *Flow of Gases through Porous Media*. New York: Academic Press.
- Castro, G. (1969). *Liquefaction of sands*. Phd thesis, Harvard University.
- Cubrinovski, M., Rhodes, A., Ntritsos, N. & Van Ballegooy, S. (2019). System response of liquefiable deposits. *Soil Dynamics and Earthquake Engineering* **124**, No. January, 212–229, doi:10.1016/j.soildyn.2018.05.013.
- Dafalias, Y. F. & Manzari, M. T. (2004). Simple Plasticity Sand Model Accounting for Fabric Change Effects. *Journal of Engineering Mechanics* **130**, No. 6, 622–634, doi:10.1061/(ASCE)0733-9399(2004)130:6(622).
- Dafalias, Y. F. & Taiebat, M. (2016). SANISAND-Z: zero elastic range sand plasticity model. *Géotechnique* **66**, No. 12, 999–1013, doi:10.1680/jgeot.15.p.271.
- Dobry, R., Ladd, R., Yokel, F., Chung, R. & Powell, R. (1982). *Prediction of Pore Water Pressure Buildup and Liquefaction of Sands During Earthquakes By the Cyclic Strain Method*. Washington, DC: National Bureau of Standards, Building Science Series 138, doi:10.6028/NBS.BSS.138.
- Elgamal, A., Yang, Z. & Lu, J. (2006). Cyclic1D: A Computer Program for Seismic Ground Response. In *Report No. SSRP-06/05*, Department of Structural Engineering, University of California, San Diego, La Jolla, CA.
- Eliadorani, A. & Vaid, Y. P. (2005). Liquefaction of Dilating Sand. In *Earthquake Engineering and Soil Dynamics*, Reston, VA: American Society of Civil Engineers, pp. 1–11, doi:10.1061/40779(158)29.
- Goren, L., Aharonov, E., Sparks, D. W. & Toussaint, R. (2010). Pore pressure evolution in deforming granular material: A general formulation and the infinitely stiff approximation. *Journal of Geophysical Research: Solid Earth* **115**, No. 9, 1–19, doi:10.1029/2009JB007191.
- Hill, R. (1958). A general theory of uniqueness and stability in elastic-plastic solids. *Journal of the Mechanics and Physics of Solids* **6**, No. 3, 236–249, doi:10.1016/0022-5096(58)90029-2.
- Ishihara, K. (1985). Stability of natural deposits during earthquakes. In *11th international conference on soil mechanics and foundation engineering*, San Francisco, USA: Balkema.
- Ishihara, K. (1993). Liquefaction and flow failure during earthquakes. *Géotechnique* **43**, No. 3, 351–451, doi:10.1680/geot.1993.43.3.351.
- Ishihara, K., Tatsuoka, F. & Yasuda, S. (1975). Undrained deformation and liquefaction of sand under cyclic stresses. *SOILS AND FOUNDATIONS* **15**, No. 1, 29–44, doi:10.3208/sandf1972.15.29.
- Kokusho, T. (1999). Water Film in Liquefied Sand and Its Effect on Lateral Spread. *Journal of Geotechnical and Geoenvironmental Engineering* **125**, No. 10, 817–826, doi:10.1061/(ASCE)1090-0241(1999)125:10(817).
- Kokusho, T. (2013). Liquefaction potential evaluations: energy-based method versus stress-based method. *Canadian Geotechnical Journal* **50**, No. 10, 1088–1099, doi:10.1139/cgj-2012-0456.
- Konrad, J. M. (1993). Undrained response of loosely compacted sands during monotonic and cyclic compression tests. *Géotechnique* **43**, No. 1, 69–89, doi:10.1680/geot.1993.43.1.69.
- Konstadinou, M. & Georgiannou, V. N. (2014). Prediction of pore water pressure generation leading to liquefaction under torsional cyclic loading. *Soils and Foundations* **54**, No. 5, 993–1005, doi:10.1016/j.sandf.2014.09.010.
- Kozeny, J. (1927). Ueber kapillare Leitung des Wassers im Boden. *Sitzungsberichte der Kaiserlichen Akademie der Wissenschaften* **136**, No. 2a, 271–306.
- Lade, P. V. (1992). Static Instability and Liquefaction of Loose Fine Sandy Slopes. *Journal of Geotechnical Engineering* **118**, No. 1, 51–71, doi:10.1061/(asce)0733-9410(1992)118:1(51).
- Lakeland, D. L., Rechenmacher, A. & Ghanem, R. (2014). Towards a complete model of soil liquefaction: the importance of fluid flow and grain motion. *Proceedings of the Royal Society A: Mathematical, Physical and Engineering Sciences* **470**, No. 2165, 20130453–20130453, doi:10.1098/rspa.2013.0453.

- Lee, K. L. & Albaisa, A. (1974). Earthquake Induced Settlements in Saturated Sands. *Journal of the Geotechnical Engineering Division* **100**, No. 4, 387–406, doi:10.1061/AJGEB6.0000034.
- Luong, M. & Sidaner, J. (1981). Undrained Behaviour of Cohesionless Soils under Cyclic and Transient Loading. *Proceedings of the First International Conference on Recent Advances in Geotechnical Earthquake Engineering and Soil Dynamics*, 215–220.
- Malvick, E., Kutter, B., Boulanger, R. & Feigenbaum, H. (2004). Post-shaking failure of sand slope in centrifuge test. In *11th Int. Conf. Soil Dynamics and Earthquake Engineering, and 3rd Int. Conf. Earthquake Geotechnical Engineering* (Doolin, D., ed.), 2, Berkeley, California, USA.: Stallion Press, pp. 447–455.
- Malvick, E. J., Kutter, B. L. & Boulanger, R. W. (2008). Postshaking Shear Strain Localization in a Centrifuge Model of a Saturated Sand Slope. *Journal of Geotechnical and Geoenvironmental Engineering* **134**, No. 2, 164–174, doi:10.1061/(ASCE)1090-0241(2008)134:2(164).
- Nemat-Nasser, S. & Shokooh, A. (1979). A unified approach to densification and liquefaction of cohesionless sand in cyclic shearing. *Canadian Geotechnical Journal* **16**, No. 4, 659–678, doi: 10.1139/t79-076.
- Nicot, F., Daouadji, A., Hadda, N., Jrad, M. & Darve, F. (2013). Granular media failure along triaxial proportional strain paths. *European Journal of Environmental and Civil Engineering* **17**, No. 9, 777–790, doi:10.1080/19648189.2013.819301.
- Pestana, J. M. & Whittle, A. J. (1995). Compression model for cohesionless soils. *Géotechnique* **45**, No. 4, 611–631, doi:10.1680/geot.1995.45.4.611.
- Prevost, J. H. (1985). A simple plasticity theory for frictional cohesionless soils. *International Journal of Soil Dynamics and Earthquake Engineering* **4**, No. 1, 9–17, doi:10.1016/0261-7277(85)90030-0.
- Seed, H. B., Idriss, I. M. & Arango, I. (1983). Evaluation of Liquefaction Potential Using Field Performance Data. *Journal of Geotechnical Engineering* **109**, No. 3, 458–482, doi:10.1061/(ASCE)0733-9410(1983)109:3(458).
- Seed, H. B. & Idriss, L. M. (1967). Analysis of Soil Liquefaction: Niigata Earthquake. *Journal of the Soil Mechanics and Foundations Division* **93**, No. SM3, 83–108.
- Seed, H. B. & Lee, K. L. (1966). Liquefaction of Saturated Sands During Cyclic Loading. *Journal of the Soil Mechanics and Foundations Division* **92**, No. 6, 105–134.
- Sivathayalan, S. & Logeswaran, P. (2008). Experimental assessment of the response of sands under shear–volume coupled deformation. *Canadian Geotechnical Journal* **45**, No. 9, 1310–1323, doi:10.1139/T08-068.
- Tasiopoulou, P. & Gerolymos, N. (2015). Constitutive modelling of sand : a progressive calibration procedure accounting for intrinsic and stress-induced anisotropy. *Geotechnique* **66**, No. 9, 754–770, doi:10.1680/jgeot.15.P.284.
- Trausch-Giudici, J. L. (2004). *Stress-strain characterisation of Seebodenlehm*. Ph.D. thesis, ETH Zurich, doi: 10.3929/ethz-a-004836423.
- Tsaparli, V., Kontoe, S., Taborda, D. M. & Potts, D. M. (2020). A case study of liquefaction: Demonstrating the application of an advanced model and understanding the pitfalls of the simplified procedure. *Geotechnique* **70**, No. 6, 538–558, doi:10.1680/jgeot.18.P.263.
- Vaid, Y. & Eliadorani, A. (2000). Undrained and drained (?) stress-strain response. *Canadian Geotechnical Journal* **37**, No. 5, 1126–1130, doi:10.1139/cgj-37-5-1126.
- Zienkiewicz, O. C., Chang, C. T. & Bettess, P. (1980). Drained, undrained, consolidating and dynamic behaviour assumptions in soils. *Géotechnique* **30**, No. 4, 385–395, doi:10.1680/geot.1980.30.4.385.